

光学学报

基于空芯反谐振光纤的三芯结构宽带耦合器设计

陈乐, 陈明阳*

江苏大学机械工程学院, 江苏 镇江 212000

摘要 提出一种基于三芯结构空芯反谐振光纤的太赫兹耦合器。采用有限元分析法对太赫兹光纤的模式特性进行分析, 并基于耦合理论得到其耦合特性曲线。仿真结果表明, 三芯结构模式具有比单芯结构更低的传输损耗, 其耦合长度可通过改变纤芯间隔和隔离包层管的间隙进行调节。采用长度为 223.2 mm 的三芯结构空芯光纤可以实现插入损耗小于 3.5 dB、带宽达到 0.52 THz 的宽带、均匀分束。

关键词 光学器件; 空芯太赫兹光纤; 反谐振; 模式耦合; 损耗特性; 带宽分析

中图分类号 TN253

文献标志码 A

DOI: 10.3788/AOS231871

1 引言

太赫兹波是指波长在 0.03~3 mm 范围内、频率为 0.1~10 THz 的电磁波, 太赫兹波的波长范围使它在短波段和长波段分别与红外波段和毫米波段重叠, 因此它成为微光子学和宏观电子学的纽带。相对于其他波段, 太赫兹波有着良好的安全性、穿透性、宽带性、相干性等优点, 在天文地理、无损检测、军事安全和生物医学等领域^[1-3], 太赫兹波的发展和研究都有着广阔前景。

太赫兹波在自由空间中的传输易受空气中的水汽等吸收的影响^[4], 为实现对太赫兹波传输的有效控制, 人们采用光纤结构传输太赫兹波。太赫兹光纤分为实芯光纤^[5]和空芯光纤^[6]两大类, 其中基于反谐振原理的空芯太赫兹光纤^[7-8]可以将太赫兹波限制在空气纤芯中传输, 极大地降低了材料吸收的影响, 受到人们的广泛关注。

在近红外波段, 光纤耦合器是实现对光进行分束、传输控制的关键器件^[9]。太赫兹耦合器是实现对太赫兹波进行分束和合束的重要器件。2010年, Nielsen 等^[10]提出一种工作在太赫兹波段的 3 dB 宽带光纤耦合器, 在两个纤芯中引入亚波长空气孔结构, 以有效提升该耦合器的带宽, 但器件的吸收损耗较大。2011年, Chen 等^[11]提出了基于三芯光子晶体光纤结构的太赫兹定向耦合器, 通过采用超小尺寸的光纤结构, 可以有效地减少由波导材料吸收引起的器件损耗。2012年, 白晋军等^[12]设计了一种基于太赫兹双芯光子带隙光纤的偏振分束器, 该偏振分束器的耦合长度小于 15 cm。2017年, Wu 等^[13]提出一

种太赫兹宽带耦合器, 该耦合器通过耦合线调整结构, 在频率为 1.47~2.3 THz 时, -10 dB 阻抗带宽为 44%, 证明了该耦合器具有优越的宽带性能。2020 年, Dinani 等^[14]提出一种基于石墨烯的太赫兹定向耦合器, 通过对石墨烯定向耦合器的耦合系数进行调整, 可以获得很好的耦合效果。2021 年, Zhu 等^[15]提出一种太赫兹光纤定向耦合器, 该定向耦合器具有对称的双悬芯结构, 可以实现低损耗和偏振不敏感的定向耦合分束。理想的耦合器应具有宽带宽、低插入损耗等特性。由于太赫兹光纤中存在吸收损耗, 太赫兹光纤耦合器的插入损耗通常较大, 从而影响其使用。基于空芯结构的太赫兹光纤虽然传输损耗较低, 但在耦合器的设计上较为困难, 更难以实现宽带分束。

本文提出一种基于三芯对称结构的空芯反谐振光纤耦合器, 利用其结构的对称性来实现宽带的分束, 并通过空芯结构有效降低耦合器的传输损耗。采用有限元法对其模式和耦合特性进行分析, 得到其耦合长度与光纤结构参数的关系, 并对其模式损耗特性进行分析, 进而获得具有低损耗和宽带宽的分束结构。

2 耦合器结构原理

图 1(a)为一种空芯反谐振光纤的横截面结构示意图, 紫色部分表示高折射率介电层, 灰色部分为空气。6 个包层管排列在光纤内, 作为单芯空芯反谐振光纤结构的基本单元。理论上, 采用双芯光纤即可实现分束, 但由于双芯结构耦合器的工作频率带宽较窄, 在传输过程中输出的光没有对称性, 很难获得均

收稿日期: 2023-12-01; 修回日期: 2024-01-03; 录用日期: 2024-01-24; 网络首发日期: 2024-02-20

通信作者: *miniyoung@163.com

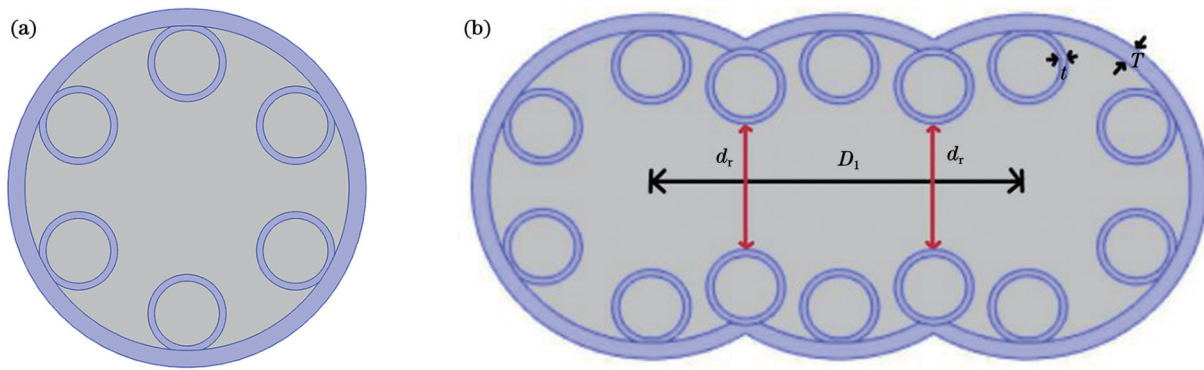


图1 空芯反谐振光纤的横截面结构示意图。(a)单芯结构;(b)三芯结构

Fig. 1 Schematic of cross-sectional structure of air-core anti-resonant fiber. (a) Single-core structure; (b) three-core structure

分输出光。因此,本文提出一种三芯光纤耦合方案,如图1(b)所示。三芯结构由图1(a)所示的单芯结构组成,相当于将3个单芯结构拼接起来,为了实现纤芯间模式的耦合,对相邻纤芯共用的空气孔位置进行微调,14个包层管排列在3个单芯空芯结构内。三芯空芯反谐振光纤的包层管在3个单芯空芯结构内部排列调整,当调整距离较短时,包层管发生相互接触,相互接触的点成为节点。由于包层管节点的存在,光纤导光传输过程中会产生Fano共振,导致光纤损耗增大^[16]。为了避免这一现象的发生,选取无节点型反谐振光纤,即包层管之间相互不接触。适当调节包层管位置,其中相邻纤芯共用的4个空气孔与其他包层管的结构参数均相同,利用这4个空气孔物理隔离此三芯结构,防止3个单芯光纤组合重叠成一个纤芯而影响耦合效果,其余包层管分布在光纤内[图1(b)]。

采用基于有限元法的商用软件COMSOL来模拟仿真所提出的空芯反谐振光纤的模式特性,使用完美匹配层(PML)^[17]来吸收辐射到边界的能量,从而减少边界处的能量反射。选取圆形作为三芯空芯反谐振光纤的完美匹配层,以减少传输过程中的损耗。为了在模拟中获得更高的精度,将模型的网格设置为波长控制,电介质区域的最大单元尺寸设置为 $\lambda/6$,空气区域的最大单元尺寸设置为 $\lambda/4$ 。

太赫兹空芯反谐振光纤的传输损耗由束缚损耗和吸收损耗组成,束缚损耗(γ_{CL})的计算公式可由复基模指数的虚部表示,即

$$\gamma_{\text{CL}} = \left(\frac{20}{\ln 10} \right) \left(\frac{2\pi}{\lambda} \right) \text{Im } n_{\text{eff}}, \quad (1)$$

式中: λ 为入射光波长; $\text{Im } n_{\text{eff}}$ 为模式的有效折射率虚部。

吸收损耗(γ_{AL})的计算过程较为繁琐,为方便计算,通过在材料的设置中引入材料的虚部得到复基模指数,将复基模指数的虚部代入式(1),得到的损耗为束缚损耗和吸收损耗之和,即模式的总损耗,将总损耗减去束缚损耗得到吸收损耗。

根据超模理论,三芯光纤耦合器支持3个超模式:2个对称模式和1个反对称模式。以模式电场的y分量 $E_y(x, y)$ 为例,如果3个超模式的有效折射率 n_{eff1} 、 n_{eff2} 、 n_{eff3} 满足

$$n_{\text{eff1}} - n_{\text{eff3}} = n_{\text{eff3}} - n_{\text{eff2}}, \quad (2)$$

即

$$2n_{\text{eff3}} - n_{\text{eff2}} - n_{\text{eff1}} = 0, \quad (3)$$

则三芯光纤耦合器中左侧A波导与右侧C波导之间会发生周期性交换,交换周期即为耦合长度 L_c ,可以表示为

$$L_c = \lambda / [2(n_{\text{eff1}} - n_{\text{eff3}})]. \quad (4)$$

这说明,利用三芯反谐振光纤在传播过程中的对称模s和反对称模a的有效折射率就可以得到该光纤的耦合长度。

单芯空芯反谐振光纤的基本参数为:纤芯直径 $D_{\text{core}}=4.37 \text{ mm}$,包层管半径 $R=0.437 \text{ mm}$,包层管介质层厚度 $t=0.09 \text{ mm}$ 。光纤材料选取环烯烃聚合物共聚物(COC),这种材料在太赫兹波导中传输的损耗和色散较低。在0.2~1.5 THz范围内,材料折射率为1.53,材料的吸收系数随频率线性增加,斜率为 $0.32 \text{ cm}^{-1}/\text{THz}$ ^[18],总体吸收系数较低。当频率为1 THz时,其模场如图2所示,束缚损耗为0.116 dB/m,吸收损耗为0.164 dB/m,传输总损耗为0.28 dB/m。可见,束缚损耗和吸收损耗相近,且吸收损耗占比更大。

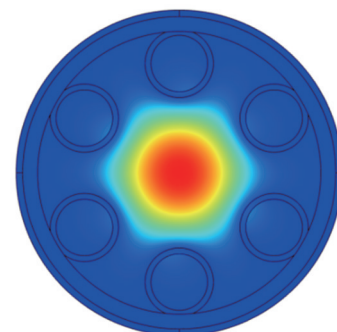


图2 空芯反谐振光纤的模场分布
Fig. 2 Mode field distribution of air-core anti-resonant fiber

3 耦合器特性分析

3.1 纤芯间距 D_1 对结构的影响

在1 THz频率下,分析纤芯间距 D_1 对耦合长度及损耗的影响。通过减少 D_1 将3个纤芯不断靠近,减小间隔纤芯孔与其相邻孔的间距,同时保持其他孔的间距和结构不变。图3所示为 $D_1=4.8$ mm时三芯结构中的模场分布。由图3可知,此结构可形成两个超模。

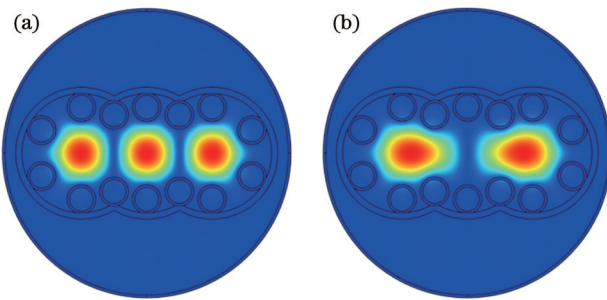


图3 $D_1=4.8$ mm时三芯结构的模场分布。(a)偶模模式;(b)奇模模式

Fig. 3 Mode field distribution for three-core configuration with $D_1=4.8$ mm. (a) Even-mode; (b) odd-mode

图4所示为 D_1 与耦合长度的关系曲线,耦合长度随着纤芯间距 D_1 的增加而增大。这是因为随着纤芯间距 D_1 的增大,相邻纤芯的模场重叠区域减小,导致耦合长度增大。需要注意的是,当纤芯间距 D_1 小于4.8 mm

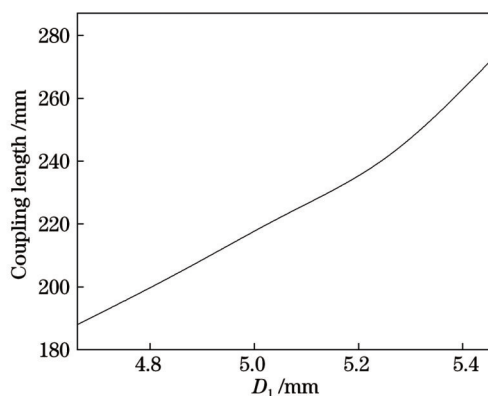


图4 D_1 与耦合长度的变化关系

Fig. 4 Relationship between D_1 and coupling length

时,3个纤芯的模式向着结构中心偏移,进而发生重叠,无法实现分束效果,因此取 $D_1 \geq 4.8$ mm。图5(a)所示为 D_1 与束缚损耗的关系曲线,由于偶模模式向中间纤芯扩展得较多, D_1 的增大造成模场增大以及纤芯束缚能力增强,束缚损耗降低,而奇模受 D_1 的影响较小。图5(b)所示为 D_1 与吸收损耗的关系曲线。从图5(c)可以看出,随着 D_1 的增大,偶模的总损耗呈现明显下降趋势,而奇模的总损耗变化不明显。与单芯光纤的模式损耗相比,三芯结构的奇模总损耗总是小于单芯结构的模式总损耗,而当 $D_1 > 4.8$ mm时,三芯结构的模式总损耗也小于单芯光纤的模式总损耗。因

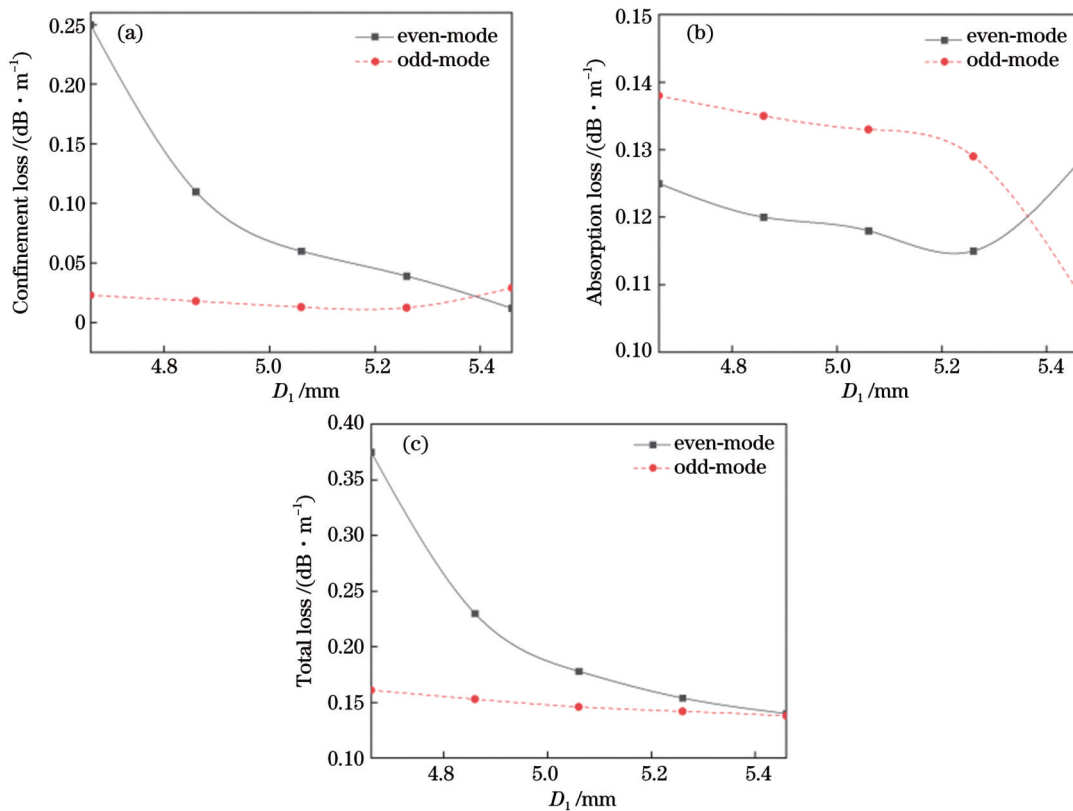


图5 D_1 与损耗的关系。(a)束缚损耗;(b)吸收损耗;(c)总损耗

Fig. 5 Relationship between D_1 and loss. (a) Confinement loss; (b) absorption loss; (c) total loss

此,采用三芯结构实际上可以获得更小的模式损耗。这也与相关理论相符,即纤芯尺寸越大,模式损耗越低^[19]。

3.2 隔离孔间距 d_r 对结构的影响

本节分析隔离孔间距对耦合长度及模式损耗的影响。根据3.1节的分析结果,将间距固定为 $D_1=5.06\text{ mm}$ 。定义两个隔离孔中心的距离为 d_s ,则孔间距 $d_r=d_s-2R$,其中 R 为隔离孔半径,如图1(b)所示。

固定频率为1 THz,分析隔离孔间距 d_r 对耦合长度及损耗的影响。当隔离孔间距大于1.9 mm时,三芯之间发生重叠,隔离孔不再进行物理隔离;当隔离孔间距小于1.0 mm时,三芯之间的耦合程度较弱,均无法实现分束效果。由图6可知:当 d_r 值较小时,其耦合长度随 d_r 的增大而缓慢下降;随着 d_r 的增大,耦合长度呈线性下降。当 $d_r=1.766\text{ mm}$ 时,纤芯间发生耦合的长度为223 mm。

图7(a)所示为 d_r 与束缚损耗的关系曲线,可以看出,束缚损耗值较低。由于奇模模场向中间纤芯扩展得较多,因此 d_r 的增加更容易增大其模场,从而减小模式的束缚损耗,而偶模模场相对独立于各纤芯, d_r 的变化对模场的影响较小。不同 d_r 值下吸收损耗的变化关系如图7(b)所示,随着 d_r 的增大,吸收损耗呈明显的下降趋势,这是因为孔间距 d_r 增大后,光纤的纤芯面积进一步增大,从而使模场向纤芯集中,其在介质材料中

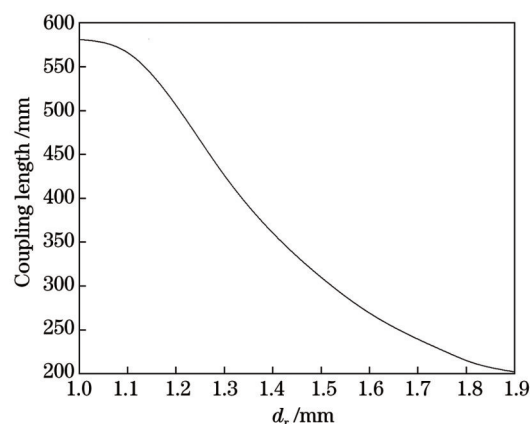


图6 d_r 与耦合长度的关系

Fig. 6 Relationship between d_r and coupling length

的比例降低,因此吸收损耗减小。对比束缚损耗和吸收损耗曲线可知,吸收损耗值明显大于相同隔离孔间距下的束缚损耗,说明模式的总损耗主要由吸收损耗决定。从图7(c)可看出,随着间距 d_r 的增大,奇模的总损耗呈明显下降趋势,而偶模的总损耗主要在 d_r 值较小时降低,随着 d_r 值的进一步增大,其对总损耗的影响逐渐变小。 $d_r=1.1\sim1.4\text{ mm}$ 时,总损耗值非常接近,波动区间为 $0.18\text{ dB/m}\sim0.25\text{ dB/m}$ 。由上述分析可知,由于三芯结构耦合器的耦合长度较短,且模式损耗较低,这种结构容易实现低损耗分束。

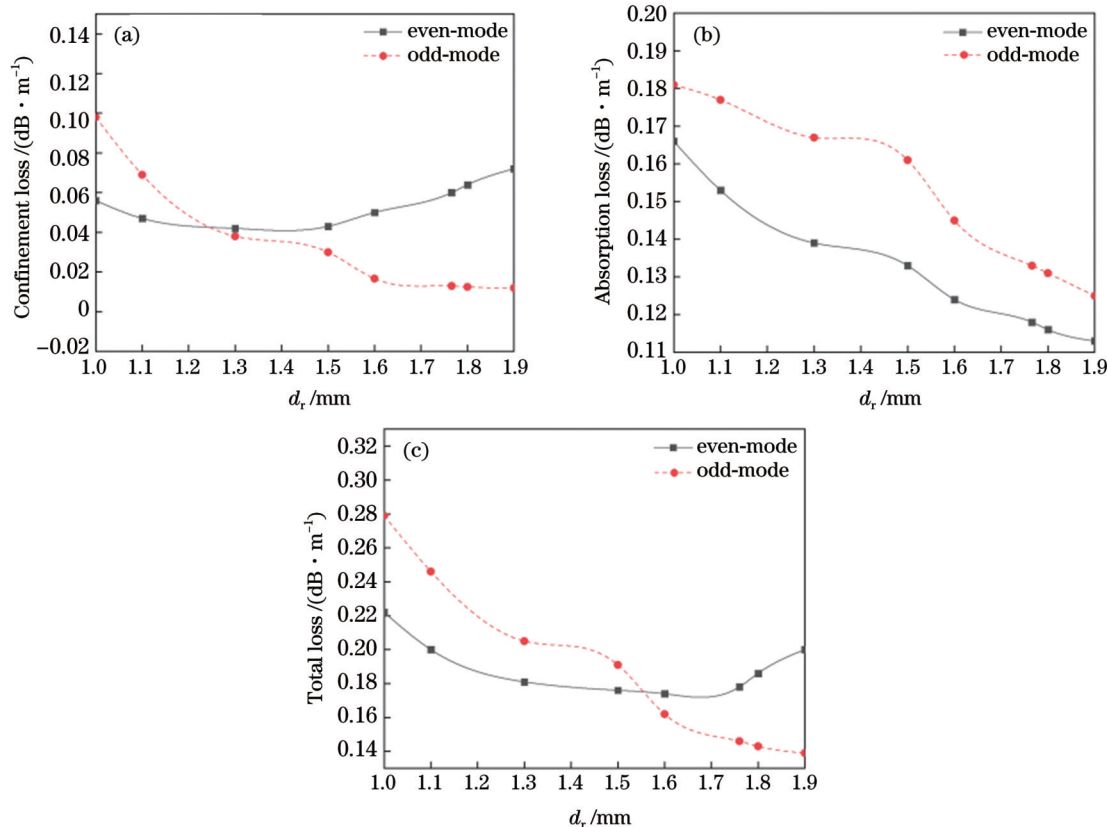


图7 d_r 与损耗的关系。(a)束缚损耗;(b)吸收损耗;(c)总损耗

Fig. 7 Relationship between d_r and loss. (a) Confinement loss; (b) absorption loss; (c) total loss

3.3 带宽分析

研究三芯空芯反谐振光纤的带宽特性。在理想情况下,输出光功率与传输距离 z 和耦合长度 L_c 的关系式为

$$P_{\text{out}} = P_{\text{in}} \cos^2 \left(\frac{\pi}{2} \cdot \frac{z}{L_c} \right), \quad (5)$$

式中: P_{out} 为输出光功率; P_{in} 为入射光功率。

考虑到模式损耗的影响,输出光功率与传输距离和耦合长度的关系式为

$$P_{\text{out1}} = P_{\text{in}} \gamma_{\text{TL}} \cos^2 \left(\frac{\pi}{2} \cdot \frac{z}{L_c} \right), \quad (6)$$

式中: γ_{TL} 为模式总损耗。

由前述分析可知,取 $D_1=5.06$ mm、 $d_r=1.766$ mm时,模式总损耗 $\gamma_{\text{TL}}=0.162$ dB。根据式(6),考虑模式传输损耗的影响,输出光功率与传输距离和耦合长度的关系曲线如图8所示。

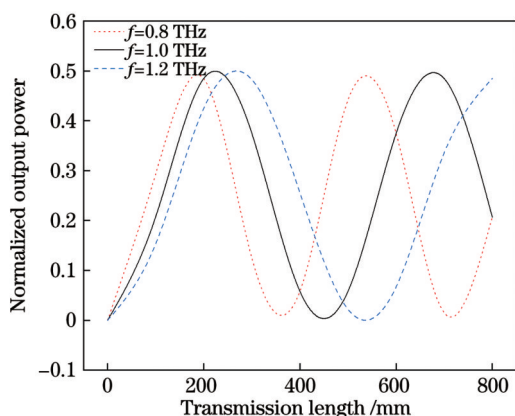


图8 侧芯中模式传输曲线

Fig. 8 Transmission curves at the side core of three-core configuration

插入损耗 a_i 是指光纤输出端口的输出光功率与输入端口的入射光功率的比值,单位为分贝(dB),计算公式为

$$a_i = -10 \log \frac{P_{\text{out}}}{P_{\text{in}}} \circ \quad (7)$$

这里取1 THz下的耦合长度为器件长度,即器件长度为223.2 mm。由式(6)得到不同频率下的输出光功率,再由式(7)得到不同频率下的插入损耗值。从图8所示的传输曲线可以看出,分束出现在传输曲线斜率值很小的位置,因此这种耦合器的带宽比较大。从插入损耗随频率的变化曲线可以得到耦合器的工作带宽,在理想情况下,1×2耦合器的插入损耗为3.0 dB。当入射波长偏离中心波长时,插入损耗会随着偏离程度的增大而增大。本研究以插入损耗小于3.5 dB为工作频率范围的限定条件。

从图9可以看出: X 偏振和 Y 偏振两种情况下,在1.0 THz附近,此结构的插入损耗均较低,1.0 THz时的最低插入损耗为3.01 dB;在所有带宽范围内,偏振

相关损耗均低于0.2 dB。从两条偏振曲线可以看出,该耦合器件对偏振不敏感,在0.82~1.34 THz范围内插入损耗均小于3.5 dB,带宽可以达到0.52 THz。综上,这种耦合器具有大带宽、低损耗传输的特点。此外,图9中仅给出一个端口的损耗曲线,由于结构具有对称性,两个端口的输出实际上是完全相同的。耦合器输出端口的宽带均匀分束特性主要源自其对称的分束结构。从图10可以看出,传输损耗对器件损耗的影响较小,与单芯结构的传输损耗相比,三芯结构的传输损耗较小。

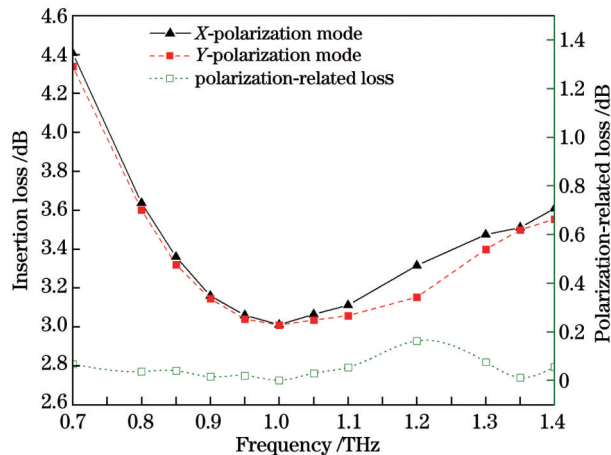


图9 插入损耗频谱曲线

Fig. 9 Insertion losses as functions of frequency

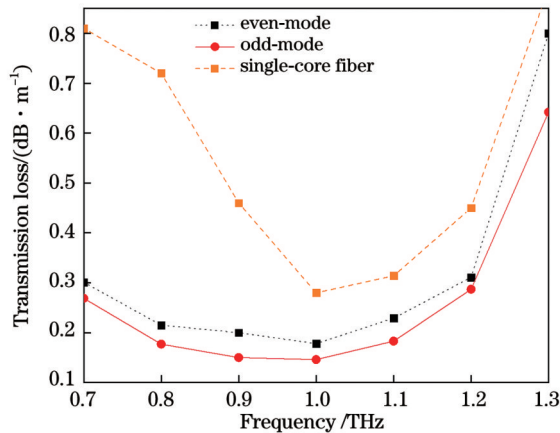


图10 三芯结构的模式传输损耗曲线

Fig. 10 Transmission loss of the even and odd modes in three-core structure

下面分析双芯结构的损耗和带宽特性。为方便结果对比,将双芯耦合器的结构参数设置成与三芯耦合器结构参数一致,即波导直径 $D_{\text{core}}=4.37$ mm,包层管半径 $R=0.437$ mm,包层管壁厚度 $t=0.09$ mm, $D_1=2.53$ mm, $d_r=1.766$ mm,双芯结构如图11所示。取中心频率为1 THz,采用前述方法可以得到其对应的耦合长度为59.28 mm。再以此光纤长度分析不同频率下两个纤芯的插入损耗。双芯耦合器两个纤芯的输出

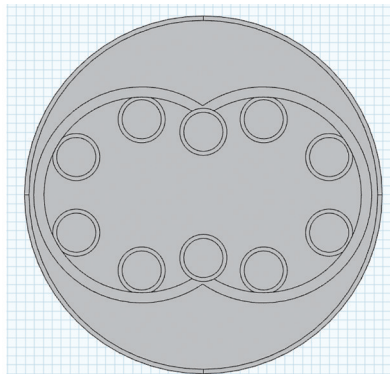


图 11 双芯结构示意图

Fig. 11 Diagram of two-core structure

能量相等,从图 12 所示的频率和插入损耗之间的关系可以看出,两个纤芯的能量处于互补的状态,在 1 THz 下左边纤芯与右边纤芯的插入损耗值均在 3 dB 附近,此时关系曲线斜率相对较大,说明插入损耗随频率的变化很快。在 0.9~1.1 THz 范围内,双芯耦合器的插入损耗小于 3.45 dB,带宽为 0.2 THz。在此频率范围内,两个输出端口的输出功率仅在 1 THz 时相同,其他位置均无法实现均匀输出。由以上结果可知,采用三芯结构可以有效增大工作带宽,且两个输出端面具有均匀输出。

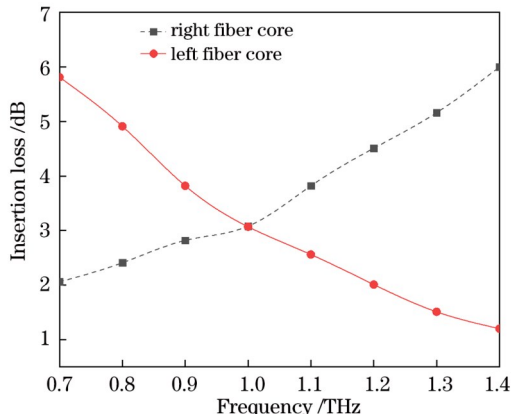


图 12 双芯结构耦合器的插入损耗曲线

Fig. 12 Insertion losses as functions of frequency for two-core structure

4 结 论

设计了一种以环烯烃共聚物为基底材料的三芯空芯反谐振太赫兹光纤耦合器,通过 COMSOL 多物理场仿真耦合软件对新型结构的太赫兹波导模式进行分析计算,对波导间的模场分布和纤芯之间模式耦合特性进行分析。采用有限元分析法和全矢量光束传播法对结构参数、耦合长度及损耗、带宽等特性进行分析。结果表明:耦合长度随着芯间距的增加而增大,随着孔间距的增大而减少,模式的传输损耗对器件插入损耗的影响很小;三芯结构由于具有对称性,可以实现均匀分光的 1×2 光分束,工作带宽达到 0.52 THz,且插入损耗小于 3.5 dB,偏振相关损耗小于 0.2 dB。

参 考 文 献

- [1] 王与烨,李海滨,葛梅兰,等.太赫兹成像技术及其应用[J].激光与光电子学进展,2023,60(18): 1811004.
Wang Y Y, Li H B, Ge M L, et al. Terahertz imaging technology and its application[J]. Laser & Optoelectronics Progress, 2023, 60(18): 1811004.
- [2] 刘晓松,赵国忠,屈媛.四种肠胃药品的太赫兹光谱实验分析[J].激光与光电子学进展,2023,60(23): 2330001.
Liu X S, Zhao G Z, Qu Y. Terahertz spectroscopy experimental analysis of four gastrointestinal drugs[J]. Laser & Optoelectronics Progress, 2023, 60(23): 2330001.
- [3] Li W P, Yu J J, Zhu B W, et al. Photonics 60 GBaud PDM-16QAM fiber-wireless 2×2 MIMO delivery at THz-band[J]. Chinese Optics Letters, 2023, 21(7): 073901.
- [4] 连想,张明浩,王国阳,等.太赫兹液体光子学研究进展[J].激光与光电子学进展,2024,61(3): 0326002.
Lian X, Zhang M H, Wang G Y, et al. Research progress in terahertz liquid photonics[J]. Laser & Optoelectronics Progress, 2024, 61(3): 0326002.
- [5] 于莹莹.太赫兹波导及特性研究[D].哈尔滨:哈尔滨工程大学,2016: 5-11.
Yu Y Y. Research of terahertz waveguide and characteristics[D]. Harbin: Harbin Engineering University, 2016: 5-11.
- [6] 严世博.新型空芯反谐振光纤的设计及其应用研究[D].北京:北京交通大学,2021: 18-19.
Yan S B. Design and application of new core anti-resonance optical fiber[D]. Beijing: Beijing Jiaotong University, 2021: 18-19.
- [7] Hayes J R, Sandoghchi S R, Bradley T D, et al. Antiresonant hollow core fiber with an octave spanning bandwidth for short haul data communications[J]. Journal of Lightwave Technology, 2017, 35(3): 437-442.
- [8] 鲁文举,张鑫,朱宽,等.无节点反谐振空芯光纤 1064 nm 高功率皮秒脉冲传输[J].中国激光,2022,49(3): 0306001.
Lu W J, Zhang X, Zhu K, et al. Propagation of high-power picosecond pulse at 1064 nm using nodeless anti-resonant hollow-core fibre[J]. Chinese Journal of Lasers, 2022, 49(3): 0306001.
- [9] Joseph T, John J. Two-core fiber based mode coupler for single-mode excitation in a two-mode fiber for quasi-single-mode operation[J]. Optical Fiber Technology, 2019, 52: 101970.
- [10] Nielsen K, Rasmussen H K, Jepsen P U, et al. Broadband terahertz fiber directional coupler[J]. Optics Letters, 2010, 35(17): 2879-2881.
- [11] Chen M Y, Fu X X, Zhang Y K. Design and analysis of a low-loss terahertz directional coupler based on three-core photonic crystal fibre configuration[J]. Journal of Physics D, 2011, 44(40): 405104.
- [12] 白晋军,王昌辉,侯宇,等.太赫兹双芯光子带隙光纤定向耦合器[J].物理学报,2012,61(10): 108701.
Bai J J, Wang C H, Hou Y, et al. Terahertz dual-core photonic band-gap fiber directional coupler[J]. Acta Physica Sinica, 2012, 61(10): 108701.
- [13] Wu Y L, Qu M J, Liu Y A, et al. A broadband graphene-based THz coupler with wide-range tunable power-dividing ratios[J]. Plasmonics, 2017, 12(5): 1487-1492.
- [14] Dinani H M, Bakhtafrouz A, Maddahali M, et al. Compact, low-loss, and wideband graphene-based directional coupler in the terahertz and infrared frequency ranges[J]. Journal of the Optical Society of America B, 2020, 37(2): 329-336.
- [15] Zhu Y F, Huang X, Ke Q, et al. Low loss and polarization-

- insensitive coupling length for a terahertz fiber directional coupler with symmetric dual-suspended core structure[J]. Optics Communications, 2021, 480: 126497.
- [16] Vincetti L, Setti V. Extra loss due to Fano resonances in inhibited coupling fibers based on a lattice of tubes[J]. Optics Express, 2012, 20(13): 14350-14361.
- [17] Pureur V, Bouwmans G, Perrin M, et al. Impact of transversal defects on confinement loss of an all-solid 2-D photonic-bandgap fiber[J]. Journal of Lightwave Technology, 2007, 25(11): 3589-3596.
- [18] Nielsen K, Rasmussen H K, Adam A J L, et al. Bendable, low-loss Topas fibers for the terahertz frequency range[J]. Optics Express, 2009, 17(10): 8592-8601.
- [19] 石文娟. 基于光子晶体光纤的偏振分束器特性研究[D]. 西安: 西安邮电大学, 2019: 19-24.
Shi W J. Research on characteristics of polarization beam splitter based on photonic crystal fiber[D]. Xi'an: Xi'an University of Posts and Telecommunications, 2019: 19-24.

Design of Three-Core Structure Broadband Coupler Based on Hollow-Core Anti-Resonant Optical Fiber

Chen Le, Chen Mingyang*

School of Mechanical Engineering, Jiangsu University, Zhenjiang 212000, Jiangsu, China

Abstract

Objective The special wavelength position of terahertz waves makes them the link between microphotonics and macroscopic electronics. However, the terahertz wave transmission in free space is easily affected by the water vapor absorption in the air. The optical fiber structure is proposed to transmit terahertz waves and realize effective transmission control. Among them, the hollow-core THz fiber based on the anti-resonant principle can limit the wave transmission in the air fiber core, which greatly reduces the influence of material absorption. The optical fiber coupler is the key device for beam splitting and transmission tailoring. Due to the existence of absorption loss in THz fiber, the insertion losses of THz fiber couplers are usually large and affect their utilization. Although the transmission loss of THz fibers with hollow-core structures is low, the design of THz couplers with broadband beam splitting is generally difficult.

Methods We propose a hollow-core anti-resonant fiber coupler based on the three-core symmetry structure. By employing its structure symmetry, broadband beam splitting can be realized, and the transmission loss of the coupler can be reduced via the hollow-core structure. The mode and coupling characteristics of the coupler are analyzed by the finite element method, and the relationship between the coupling length and the fiber structure parameters is verified. The mode loss characteristics of the coupler are analyzed, and then the beam splitting structure with low loss and wide bandwidth is obtained.

Results and Discussions We design a hollow-core three-core anti-resonant fiber. At the frequency of 1 THz, the coupling length increases with the rising core distance (Fig. 4). As can be seen from the relation curve between D_1 and binding loss, since the even mode field expands more to the intermediate core, the increase in D_1 leads to the growing mode field, and the improvement in the binding ability of the core reduces the binding loss, while the odd mode is less affected by D_1 [Fig. 5(a)]. With the increasing D_1 , the total loss of even mode obviously shows a downward trend, while the change of odd mode is not obvious. Compared with the mode loss of single-core fiber, the total odd-mode loss of the three-core structure is always smaller than that of the single-core structure in the shown interval. Therefore, using the three-core structure can actually obtain smaller mode losses. This is also consistent with the theory that the larger core size leads to lower mode losses [Fig. 5(c)]. The coupling length decreases slowly with the rising d_r when the separation hole spacing d is small. As d_r spacing increases, the coupling length decreases linearly (Fig. 6). Since the odd-mode field extends more to the intermediate core, the d_r increase is easier to increase its mode field, thereby reducing the mode binding loss, while the even-mode field is relatively independent of each core, and thus the change of d_r has little effect on it [Fig. 7(a)]. With the increasing d_r , the absorption loss shows an obvious downward trend, and the total mode loss is mainly determined by the absorption loss [Fig. 7(b)]. With the rising spacing d_r , the total loss of odd mode shows an obvious downward trend, while that of even mode mainly decreases under small d_r values, and the further increase in d_r value has little influence on it [Fig. 7(c)]. The relationship between the output optical power under the influence of mode transmission loss and transmission distance and coupling length is shown in Eq. (6) and Fig. 8. In all bandwidth ranges, the polarization-related loss is lower than 0.2 dB. The two polarization curves indicate that the coupler is not sensitive to

polarization, the insertion loss is less than 3.5 dB in the range of 0.82–1.34 THz, and the bandwidth can reach 0.52 THz. This coupler is found to feature wide bandwidth and low loss transmission (Fig. 9). Transmission loss has less effect on the loss of the device (Fig. 10). The two-core coupler is in the range of 0.9–1.1 THz, the insertion loss is less than 3.45 dB, and the bandwidth is 0.2 THz. In the working bandwidth range, the two output ports cannot output the same power, and when the output power difference between the two ports is less than 0.1 dB, the corresponding bandwidth is 1 THz, with a large output power difference. The working bandwidth of the three-core structure coupler and the two-core structure coupler is relatively narrow (Fig. 12).

Conclusions We design an anti-resonant air-core three-core terahertz fiber coupler with cycloolefin copolymer as the base material. The mode analysis and calculation of the new structure of the terahertz waveguide are carried out by COMSOL multi-physics simulation coupling software, and the mode field distribution among waveguides and the mode coupling characteristics between fiber cores are analyzed. Finite element analysis and full vector beam propagation method are employed to analyze the structural parameters, coupling length and loss effects, bandwidth, and other characteristics. The results show that the coupling length increases with the rising core spacing and decreases with the growing hole spacing, and the mode transmission loss has little effect on the insertion loss of the device. Due to the symmetry, the three-core structure can realize the uniform beam splitting of 1×2 light, the working bandwidth reaches 0.52 THz, and the insertion loss is less than 3.5 dB, with the polarization-related loss less than 0.2 dB.

Key words optical devices; hollow-core THz optical fiber; anti-resonance; mode coupling; loss characteristic; bandwidth analysis